arXiv:2205.15484v1 [physics.atom-ph] 31 May 2022

Prospects of a thousand-ion Sn^{2+} Coulomb-crystal clock with sub-10^{-19} inaccuracy

David R. Leibrandt,[1, 2, *] Sergey G. Porsev,[3] Charles Cheung,[3] and Marianna S. Safronova[3]
[1] *Time and Frequency Division, National Institute of Standards and Technology, Boulder, Colorado, 80305, USA*
[2] *Department of Physics, University of Colorado, Boulder, Colorado, 80309, USA*
[3] *Department of Physics and Astronomy, University of Delaware, Newark, Delaware 19716, USA*

(Dated: June 1, 2022)

We propose a many-ion optical atomic clock based on three-dimensional Coulomb crystals of order one thousand Sn^{2+} ions confined in a linear RF Paul trap. Sn^{2+} has a unique combination of features that is not available in previously considered ions: a $^1\mathrm{S}_0 \leftrightarrow {}^3\mathrm{P}_0$ clock transition between two states with zero electronic and nuclear angular momentum (I = J = F = 0) making it immune to nonscalar perturbations, a negative differential polarizability making it possible to operate the trap in a manner such that the two dominant shifts for three-dimensional ion crystals cancel each other, and a laser-accessible transition suitable for direct laser cooling and state readout. We present analytical calculations of the differential polarizability and other relevant atomic properties, as well as numerical calculations of the motion of ions in large Coulomb crystals, to estimate the achievable accuracy and precision of Sn^{2+} Coulomb-crystal clocks.

INTRODUCTION

Optical atomic clocks based on single trapped ions and on ensembles of thousands of lattice-trapped neutral atoms have both achieved 10^{-18} fractional frequency accuracy and precision [1], surpassing the microwave atomic clocks that underpin international atomic time (TAI) by three orders of magnitude, and enabling new technological applications such as relativistic geodesy [2], as well as tests of the fundamental laws of physics [3]. For any particular application, ion and lattice optical clocks have complimentary advantages and limitations. Optical lattice clocks use simultaneous measurements of thousands of atoms to quickly down average quantum projection noise (QPN), a fundamental limit to clock precision, speeding up both characterizations of systematic effects and clock measurements, and increasing the bandwidth of sensing applications. However, they suffer from larger systematic frequency shifts due to the trapping fields and interactions between atoms that are difficult to control. Clocks based on one or a few trapped ions suffer from larger QPN, but offer exquisite control of environmental perturbations and interactions, high-fidelity universal quantum control at the individual ion level, and a wide variety of atomic, molecular, and highly-charged ions to choose from with different sensitivities to environmental perturbations and proposed extensions of the Standard Model of particle physics.

Recently, a wide variety of new optical clock platforms, which overcome some of the limitations of conventional lattice and ion clocks, have been proposed and demonstrated. Composite optical clocks combining an ensemble of lattice-trapped atoms that provides high stability, together with a single trapped ion that provides high accuracy, have been proposed [4, 5], and the fundamental building blocks have been demonstrated [6]. Ion trap arrays have been built and shown to be capable of supporting clock operation with around 100 ions and sub-10^{-18}

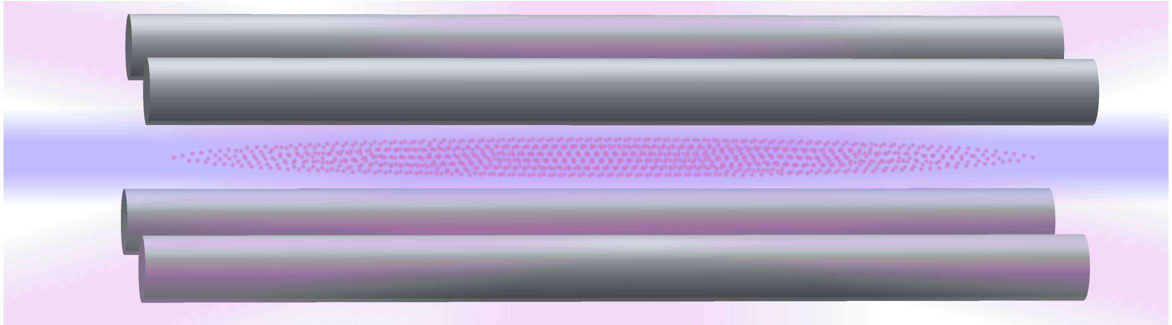

FIG. 1. Schematic of a many-ion optical atomic clock based on Sn^{2+} ions. A three-dimensional Coulomb crystal of 1000 Sn^{2+} ions (small dots) is confined in a linear RF Paul trap (grey cylindrical electrodes). For single-ion secular motional frequencies 1.15 MHz, 0.85 MHz, and 0.10 MHz, the diameters of the ellipsoidal ion crystal are 19 μm, 44 μm, and 909 μm. Sn^{2+} is laser-cooled using three orthogonal lasers (shown in pink) red-detuned from the 181 nm $^1\mathrm{S}_0 \leftrightarrow {}^3\mathrm{P}_1$ transition. Spectroscopy of the 187 nm $^1\mathrm{S}_0 \leftrightarrow {}^3\mathrm{P}_0$ clock transition is performed using a laser aligned with the axial trap direction (shown in purple), and readout is based on state-dependant photon scattering on the $^1\mathrm{S}_0 \leftrightarrow {}^3\mathrm{P}_1$ transition.

accuracy [7]. Clocks based on arrays of optical-tweezer-trapped atoms offer the prospect of individual-atom-resolved quantum control, and have demonstrated coherence times exceeding 40 s and operation with up to 150 atoms [8]. Three-dimensional optical lattice clocks greatly suppress the interactions between atoms present in current lattice clocks based on one and two-dimensional optical lattice traps and have demonstrated operation with up to 10^5 atoms [9].

Three-dimensional Coulomb crystals of thousands of ions in linear RF Paul traps have been studied for many years for other applications [10–15], however they were thought to be impractical for atomic clocks because ions located off of the trap axis, along which the RF trapping electric field is zero, suffer from driven motion called micromotion that leads to large time-dilation systematic frequency shifts. Berkeland *et al.* [16] pointed out that for clock transitions with a negative differential polarizability, the negative micromotion time-dilation shift could be almost perfectly cancelled out by a positive differential Stark-shift caused by the same RF trapping field that drives the micromotion, provided that the trap is driven at a "magic" value of the RF frequency. Building on this, Arnold *et al.* [17] proposed that many-ion clocks could be built based on three-dimensional Coulomb crystals of ions with negative-differential-polarizability clock transitions, which at the time was thought to include B^+, Ca^+, Sr^+, Ba^+, Ra^+, Er^{2+}, Tm^{3+}, and Lu^+. It was later experimentally determined that the ${}^1\mathrm{S}_0 \leftrightarrow {}^3\mathrm{D}_1$ clock transition of Lu^+ actually has a very small, but positive differential polarizability, and the alternative ${}^1\mathrm{S}_0 \leftrightarrow {}^3\mathrm{D}_2$ clock transition of Lu^+ has a negative, but relatively large differential polarizability [18], in contrast with earlier theoretical predictions. Pb^{2+} was added to this list by Beloy [19]. Of the remaining candidates for Coulomb-crystal clocks, Ca^+, Sr^+, Ba^+, Ra^+, Er^{2+}, and Tm^{3+} have electric-quadrupole clock transitions with excited-state lifetimes that limit probe durations to less than approximately 1 s. B^+ and Pb^{2+} have doubly-forbidden intercombination clock transitions with greater than 10^3 s lifetimes, but do not have transitions suitable for direct state readout and it is not known how to extend indirect quantum-logic readout [20] to large Coulomb crystals.

In this article, we propose Coulomb-crystal clocks based on up to an order of one thousand Sn^{2+} ions (see Figure 1). We present a theoretical calculation of the differential polarizability of the ${}^1\mathrm{S}_0 \leftrightarrow {}^3\mathrm{P}_0$ clock transition, showing it to be both small and negative, meaning that the systematic shift due to blackbody radiation is small, and there is a magic trap frequency of 225(5) MHz at which the trap Stark shift cancels the micromotion time-dilation shift. Similar to Pb^{2+}, in addition to having zero electronic spin in the two clock states, there are several isotopes of Sn^{2+} that have zero nuclear spin, and thus the clock transition is completely immune to nonscalar perturbations [19]. Furthermore, for these nuclear-spin-zero isotopes, the clock transition is an extremely forbidden intercombination transition with a zero-magnetic-field excited state lifetime of order of years, but the lifetime can be tuned to an experimentally convenient value by applying a magnetic quantization field. However, unlike B^+ and Pb^{2+}, Sn^{2+} has a laser-accessible ${}^1\mathrm{S}_0 \leftrightarrow {}^3\mathrm{P}_1$ transition suitable for direct laser cooling and state readout, enabling many-ion clock operation. We present analytical calculations of the Sn^{2+} atomic properties relevant for evaluation of the systematic frequency shifts as well as numerical calculations of the motion of ions in large Coulomb crystals that lead to imperfect cancellation of the micromotion time-dilation and trap Stark shift, and imperfections in the spectroscopic lineshape. It may be possible to simultaneously achieve 9.0×10^{-20} total fractional inaccuracy and $4.4 \times 10^{-18}/\tau^{1/2}$ fractional imprecision, where τ is the measurement duration in seconds. We conclude by discussing prospects for fifth force searches using isotope shift measurements, as well as other tests of fundamental physics with Sn^{2+} .

RESULTS

Sn^{2+} atomic properties. Figure 2a shows an energy level diagram of Sn^{2+}. We carried out calculations of Sn^{2+} atomic properties using a high-accuracy relativistic method combining configuration interaction (CI) with the linearized coupled-cluster approach (CI+all-order method) [21]. To evaluate uncertainties of the results, we also carried out the same calculations using a combination of the CI and many-body perturbation theory (CI+MBPT method [22]). Since the CI is essentially complete for a divalent system, the main source of the uncertainty is the treatment of the core, which is estimated as the difference between the results obtained by these two methods [23]. The results of the calculations given in Tables I and II are used to design and evaluate the performance of the Sn^{2+} clock schemes.

The $5s5p\,{}^3P_1$ state mostly decays trough the ${}^3P_1 \leftrightarrow {}^1S_0$ transition, which will be used for cooling and readout. We found this transition rate to be $7.1 \times 10^6\ \mathrm{s}^{-1}$ and, respectively, the lifetime of the ${}^3P_1$ state to be $\tau({}^3P_1) \approx$ 141 ns.

The ${}^3P_0 \leftrightarrow {}^1S_0$ clock transition is forbidden by single-photon-transition selection rules, but it can be opened in the presence of the magnetic field due to admixture of the ${}^{3,1}P_1$ states to ${}^3P_0$ by the $\boldsymbol{\mu}\mathbf{B}$ operator (where $\boldsymbol{\mu}$ is the magnetic dipole moment operator and $\mathbf{B}$ is the static magnetic field).

Restricting ourselves by the admixture of the two nearest to ${}^3P_0$ states of the same parity, $5s5p\,{}^3P_0$ and $5s5p\,{}^1P_1$, we arrive at the following expression for the ${}^3P_0 \leftrightarrow {}^1S_0$

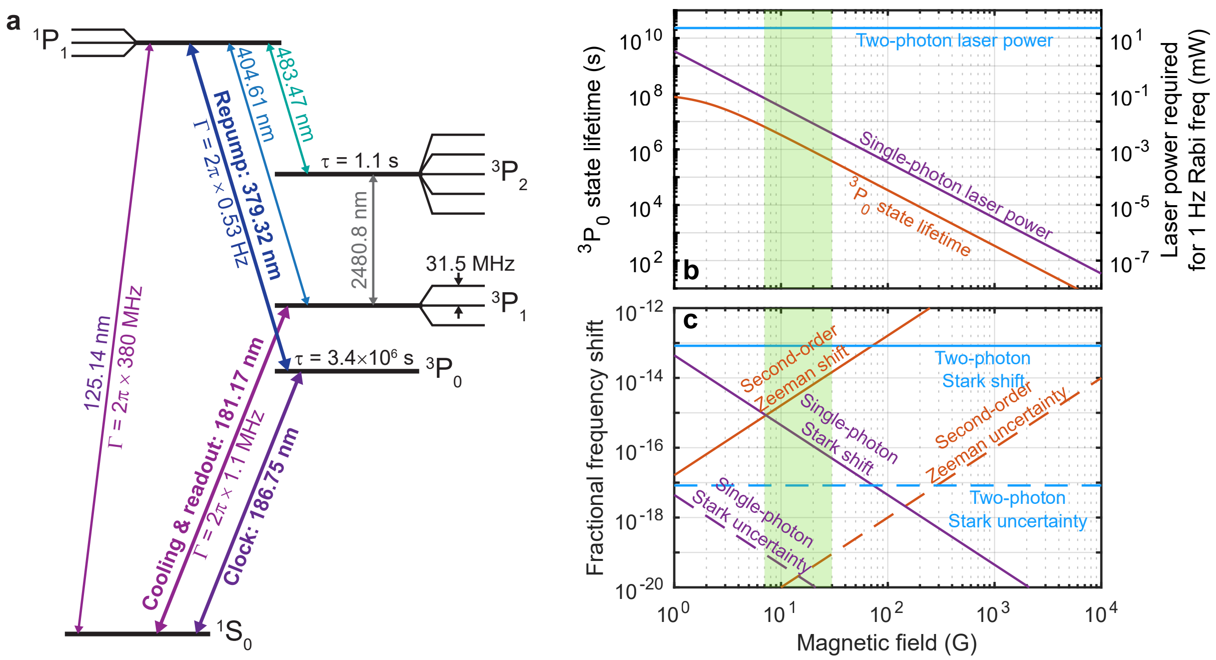

FIG. 2. Sn^{2+} atomic properties. (a) Energy level diagram showing the states and transitions relevant for clock operation using a nuclear-spin-zero isotope of Sn^{2+} at a magnetic field of 15 G. Thick horizontal black lines indicate eigenstates of the magnitude of the orbital, spin, and total angular momentum labeled by the term symbols $^{2S+1}L_J$ where the quantum number $S \in \{0, 1\}$ is the magnitude of the spin angular momentum, $L \in \{\text{S,P}\}$ is the magnitude of the orbital angular momentum, and $J \in \{0, 1, 2\}$ is the magnitude of the total angular momentum. Thin black lines indicate Zeeman splittings of the states with different values of the m quantum number, which denotes the projection of the total angular momentum on the quantization axis. (b) Lifetime of the excited clock state and the laser power required to drive the clock transition as a function of the applied magnetic field. At zero magnetic field the clock transition is highly forbidden, leading to a spontaneous emission lifetime of the excited clock state of many years and requiring high laser intensity to drive the transition. As the magnetic field is increased, the $^3P_0$ state is weakly mixed with the $^3P_1$ state, leading to a reduced $^3P_0$ lifetime and laser intensity requirement. The laser power required to drive the clock transition with a Rabi frequency $\Omega/(2\pi) = 1$ Hz is shown both for driving the transition with a single 187 nm photon and for driving it with two 374 nm photons, assuming a 100 μm $1/e^2$ laser beam diameter. (c) Systematic frequency shifts and estimated uncertainties due to the second-order Zeeman effect caused by the applied magnetic field and the Stark effect caused the laser used to drive the clock transition, as a function of the applied magnetic field.

transition rate:

$$W \approx \frac{2\omega^3}{27\varepsilon_0 h c^3} \times \left| \sum_{n={}^3P_1,{}^1P_1} \frac{\langle {}^1S_0||d||n\rangle\langle n||\mu||{}^3P_0\rangle}{E(n)-E({}^3P_0)} \right|^2 B^2, \qquad (1)$$

where ω is the $^3P_0 \leftrightarrow {}^1S_0$ transition frequency, $\mathbf{d}$ is the electric dipole operator, E is a state energy, and ε_0, $\hbar$, and c are the vacuum permittivity, Plank constant, and speed of light, respectively. We assume that the field $\mathbf{B}$ is directed along the z axis. The matrix elements of the electric and magnetic dipole operators expressed in ea_0 and μ_0 (where e is the elementary charge and a_0 and μ_0 are the Bohr radius and magneton) are given in Table I. Using Eq. (1), we find the $^3P_0$ lifetime to be $\tau(^3P_0) \approx 3.4\,(\mathrm{s\,T^2})/B^2$, where B is expressed in T. The CI+all-order values of the matrix elements and experimental energies [24] are used to compute all transition rates.

Static and dynamic polarizabilities needed for the evaluation of the blackbody radiation shift and the ac Stark shifts are listed in Table I. The blackbody radiation shift is mostly determined by the differential static polarizability of the the $5s5p\,^3P_0$ and $5s^2\,^1S_0$ clock states, $\Delta\alpha \equiv \alpha(^3P_0) - \alpha(^1S_0) \approx -0.96(4)\,a_0^3$. Based on the difference between the CI+all-order and CI+MBPT values, we determined the uncertainty of $\Delta\alpha$ at the level of 4%.

The dynamic polarizibilities of the clock states at the clock wavelengths $\lambda_0 \approx 186.75$ nm and $\lambda = 2\lambda_0 \approx 373.5$ nm are listed in Table I.

Micromotion driven by the rf-trapping field leads to ac Stark and second-order Doppler shifts. As predicted by Berkeland *et al.* [16] and demonstrated by Dub *et al.* [25], if the differential static polarizability $\Delta\alpha$ for the clock transition is negative, there is a “magic” trap drive

TABLE I. Energies (in cm^{-1}), matrix elements of the electric dipole operator (in ea_0) and magnetic dipole operator (in μ_0), and static polarizibilities of the $^3P_0$ and $^1S_0$ states and their differential polarizability $\Delta\alpha$ (in a_0^3), calculated in the CI+MBPT (labeled as "CI+MBPT") and CI+all-order (labeled as "CI+All") approximations. The energies are referenced to the ground state. Uncertainties are given in parentheses.

		CI+MBPT	CI+All	Exp. [24]
	$5s5p\,^3P_0$	55236	54083	53548
	$5s5p\,^3P_1$	56858	55707	55196
	$5s5p\,^1P_1$	80162	80166	79912
	$\langle ^3P_0\|\|\mu\|\|^3P_1\rangle$	-1.405	-1.406	
	$\langle ^3P_0\|\|\mu\|\|^1P_1\rangle$	0.151	0.141	
	$\langle ^3P_1\|\|d\|\|^1S_0\rangle$	0.268	0.249	
	$\langle ^1P_1\|\|d\|\|^1S_0\rangle$	2.639	2.640	
Static	$\alpha(^1S_0)$	15.16	15.20	
	$\alpha(^3P_0)$	14.20	14.25	
	$\Delta\alpha$	-0.96(4)	-0.96(4)	
$\lambda = 186.75$ nm	$\alpha(^1S_0)$	27.18	27.80	
	$\alpha(^3P_0)$	23.30	23.42	
	$\Delta\alpha$	-3.9	-4.4(5)	
$\lambda = 373.5$ nm	$\alpha(^1S_0)$	17.17	17.21	
	$\alpha(^3P_0)$	15.94	16.00	
	$\Delta\alpha$	-1.23	-1.21(2)	

frequency Ω_m given by

$$\Omega_m = \frac{Q_i}{M_i c}\sqrt{-\frac{\hbar\omega}{\Delta\alpha}} \qquad (2)$$

(Q_i and M_i are the ion charge and mass), at which the micromotion shift vanishes. Substituting $M_i \approx A\,m_p$ (where m_p is the proton mass and we use for an estimate $A = 118$) and $\Delta\alpha = -0.96(4)\,a_0^3$, we obtain $\Omega_m/(2\pi) = 225(5)$ MHz.

Calculations of other atomic properties relevant for clock operation are described in the Methods.

TABLE II. The reduced MEs of the electric multipole Ek operator (in ea_0^k) and magnetic multipole Mk operator (in $\mu_0\, a_0^{k-1}$), and the transition rates, W (in s^{-1}), from $5s5p\,^3P_2$ and $5s5p\,^1P_1$ to the lower-lying states, calculated in the CI+all-order+RPA approximation, are presented.

Transition	Mult.	ME	W (s^{-1})
$^3P_2 - {}^1S_0$	$M2$	11	0.03
$^3P_2 - {}^3P_0$	$E2$	5.1	0.003
$^3P_2 - {}^3P_1$	$M1$	1.6	0.87
	$E2$	7.6	0.001
$^1P_1 - {}^1S_0$	$E1$	2.6	2.4×10^9
$^1P_1 - {}^3P_0$	$M1$	0.14	3.3
$^1P_1 - {}^3P_1$	$M1$	0.12	2.0
	$E2$	1.2	0.47
$^1P_1 - {}^3P_2$	$M1$	0.16	2.0
	$E2$	0.87	0.11

Sn^{2+} clock operation. Each cycle of basic Sn^{2+} clock operation consists of four steps. First, the ions are laser cooled on the 181 nm ^{1}S$_0$ ↔ ^{3}P$_1$ transition. The $\Gamma/(2\pi) = 1.1$ MHz natural linewidth of this transition is sufficiently narrow for Doppler cooling to sub-mK temperatures, at which the fractional time-dilation shift due to secular (i.e., thermal) motion of the ions is at or below the 10^{-18} level, and can be characterized such that the uncertaintly is significantly better. It is also sufficiently broad to achieve the high cooling rates necessary for crystallization of ions initially loaded into the trap at above room-temperature in a delocalized cloud phase. For many-ion crystals with a spectrum of secular-motion normal mode frequencies spanning from tens of kHz to above 1 MHz, efficient Doppler cooling of all modes will require driving above saturation to power broaden the transition to significantly more than the motional mode bandwidth, and use of three laser beams with k-vectors that have significant overlap with all spatial directions. In the calculations below, we assume a saturation parameter of 20, such that the transition is power broadened to a linewidth of 5 MHz.

Second, spectroscopy is performed on the ^{1}S$_0$ ↔^{3}P$_0$ clock transition. This transition can be driven either as a single-photon transition using a laser at 187 nm, or as a two-photon transition using a laser at 374 nm (see Figure 2 b and c). The two-photon option has the advantages that it can be driven at or near zero applied magnetic field, which minimizes the second-order Zeeman shift, and using a photon from each of two counter-propagating beams, which eliminates motional sideband transitions, but the disadvantage that it requires high laser intensity with an associated Stark shift of order 10^{-13}. Although this can be suppressed by using hyper-Ramsey [26] or auto-balanced Ramsey [27] interrogation protocols, it may not be possible to reduce the uncertainty to below 10^{-18}. The single-photon option has the advantage that the required laser intensity can be reduced by increasing the magnetic field, but this comes at the cost of an increased second-order Zeeman shift. We estimate that at magnetic fields around 15 G, the quadrature sum of the uncertainties due to the probe-laser Stark shift and the second-order Zeeman shift can be minimized as shown in Figure 2c. With 15 μW of laser power focused to a 100 μm $1/e^2$ beam diameter, the single-photon Rabi frequency $\Omega/(2\pi) = 1$ Hz and the Stark shift is 2.0×10^{-16}. We conservatively estimate that this can be characterized to an uncertainty of 2.0×10^{-20}. The second-order Zeeman shift is -3.7×10^{-15}, and by measuring the clock transition frequency at significantly higher magnetic field, it should be possible to characterize this shift to an uncertainty of 2.3×10^{-20}. For 1000 Sn^{2+} ions in a trap with single-ion secular frequencies 1.15 MHz, 0.85 MHz, and 0.10 MHz, the diameters of the ellipsoidal ion crystal major axes are 19 μm, 44 μm, and 909 μm, and the magnetic field only needs to be homogenous at the 1 G level over this volume to avoid inhomogeneous broadening for sub-1 Hz linewidth spectroscopy.

Third, the number of ions in the ground and excited states is read out by driving the ${}^1\mathrm{S}_0 \leftrightarrow {}^3\mathrm{P}_1$ transition and counting the total number of photons scattered into a photomultiplier tube (PMT) or other detector. During a $\tau = 300$ μs detection period and assuming a total detection efficiency $\epsilon = 1$ %, up to $\epsilon\Gamma\tau/2 = 10$ photons will be detected per ion that remains in the ground state after clock interrogation. This is sufficient to suppress detection-photon shot noise below the QPN limit. The fraction of excited state ions is used to determine the frequency offset between the clock laser and the atomic transition frequency, and frequency feedback is applied to clock laser to keep it on resonance.

Fourth, the ions that are in the excited state after clock interrogation are repumped to the ground state by driving the 379 nm ${}^3\mathrm{P}_0 \leftrightarrow {}^1\mathrm{P}_1$ transition. The ${}^1\mathrm{P}_1$ state quickly decays to ${}^1\mathrm{S}_0$, with negligible branching ratios for decay to ${}^3\mathrm{P}_1$ and ${}^3\mathrm{P}_2$. Optionally, the total number of ions can be determined by performing readout again after repumping. Subsequently, the next cycle of clock operation can begin.

Many-ion clock considerations. Three-dimensional Coulomb crystals of many ions can be confined in a single linear RF Paul trap [10]. For large Coulomb crystals of a fixed number of ions, there are multiple local minima of the total zero-temperature energy consisting of the Coulomb energy due to repulsion of the ions from each other, the time-averaged Coulomb energy of the ions with the trapping fields, and the time-averaged kinetic energy of the micromotion. These local minima correspond to stable geometric crystal configurations, in which each ion is spatially localized and oscillates about its equilibrium position due to micromotion. Distinct crystal configurations have different sets of equilibrium ion positions. Different configurations are observed both theoretically [28] and experimentally [12, 29] when ions are laser cooled to a crystalline state starting from a non-localized cloud state with identical initial thermal properties. Similar to Arnold *et al.* [17], we have calculated equilibrium ion positions by time-evolving the equations of motion in the pseudopotential approximation starting from random initial positions and including a damping force that qualitatively represents laser cooling. For each set of trap parameters and number of ions investigated, we generate up to 36 configurations in parallel using a high-performance computer cluster. For ion numbers up to 1000, this takes less than one week. Once the equilibrium ion positions are known, it is straightforward to compute the frequencies and eigenvectors of the normal modes of secular motion and their Lamb-Dicke parameters [30], the amplitude and direction of micromotion of each ion (by time evolving the full time-dependent equations of motion), and the spectrum of the clock transition [31].

Figures 3a and 3b show the fractional frequency shifts due to secular motion, micromotion, and the Stark shift due to the trapping fields, averaged over all of the ions, and estimates of the uncertainties with which these shifts can be characterized. For these calculations, the trap is assumed to be driven at the magic RF frequency with voltages such that the secular frequencies of a single ion in the trap are 1.15 MHz, 0.85 MHz, and 0.10 MHz. The number of ions varies from 50 to 1000. The magnitude of the average micromotion time-dilation shift increases with the number of ions as ions are pushed further away from the trap axis, along which the AC electric field is zero, reaching 3.7×10^{-14} for 1000 ions. The time-dilation shift due to micromotion at exactly the magic trap drive frequency is perfectly cancelled by the Stark shift, due to the electric field that drives the motion, as indicated in Figure 3d. There is also a time-dilation shift due to micromotion at twice the trap drive frequency, which is not cancelled by the corresponding Stark shift, and this motion prevents perfect cancellation of micromotion time dilation [25]. The net micromotion shift after this imperfect cancellation for 1000 ions is 2.8×10^{-19}, and it should be possible to characterize this shift to achieve an uncertainty that is at least one order of magnitude smaller. Figure 3c shows a histogram of the net micromotion shifts of each ion individually; the sub-10^{-18} inhomogeneous broadening of this distribution will not limit spectroscopic coherence within the forseeable future. The net secular motion shift for 1000 ions is -2.4×10^{-19}, and we conservatively estimate that this can be characterized with an uncertainty of 7.2×10^{-20}.

Ion motion leads to motional sidebands on the clock transition and an inhomogeneous reduction of the Rabi frequency for driving the carrier transition due to the Debye-Waller factors of each ion [31, 32]. Micromotion is dominantly along the radial trap directions and its effect on the clock transition spectrum can be nearly eliminated by probing along the axial trap direction. Figure 4a shows the spectrum of the secular motional mode frequencies for a 1000 ion crystal with the same trap parameters as above. The distribution of Debye-Waller factors of each ion for axial probing due to secular motion at a temperature of 120 μK, corresponding to the Doppler cooling limit with a 5 MHz power broadened linewidth, is shown in Figure 4b. The contrast for Rabi spectroscopy of the clock transition is maximized by setting the laser intensity and pulse duration such that ions with the median value of the Rabi frequency undergo a π-pulse when the laser is on resonance. Figure 4c shows the spectrum of

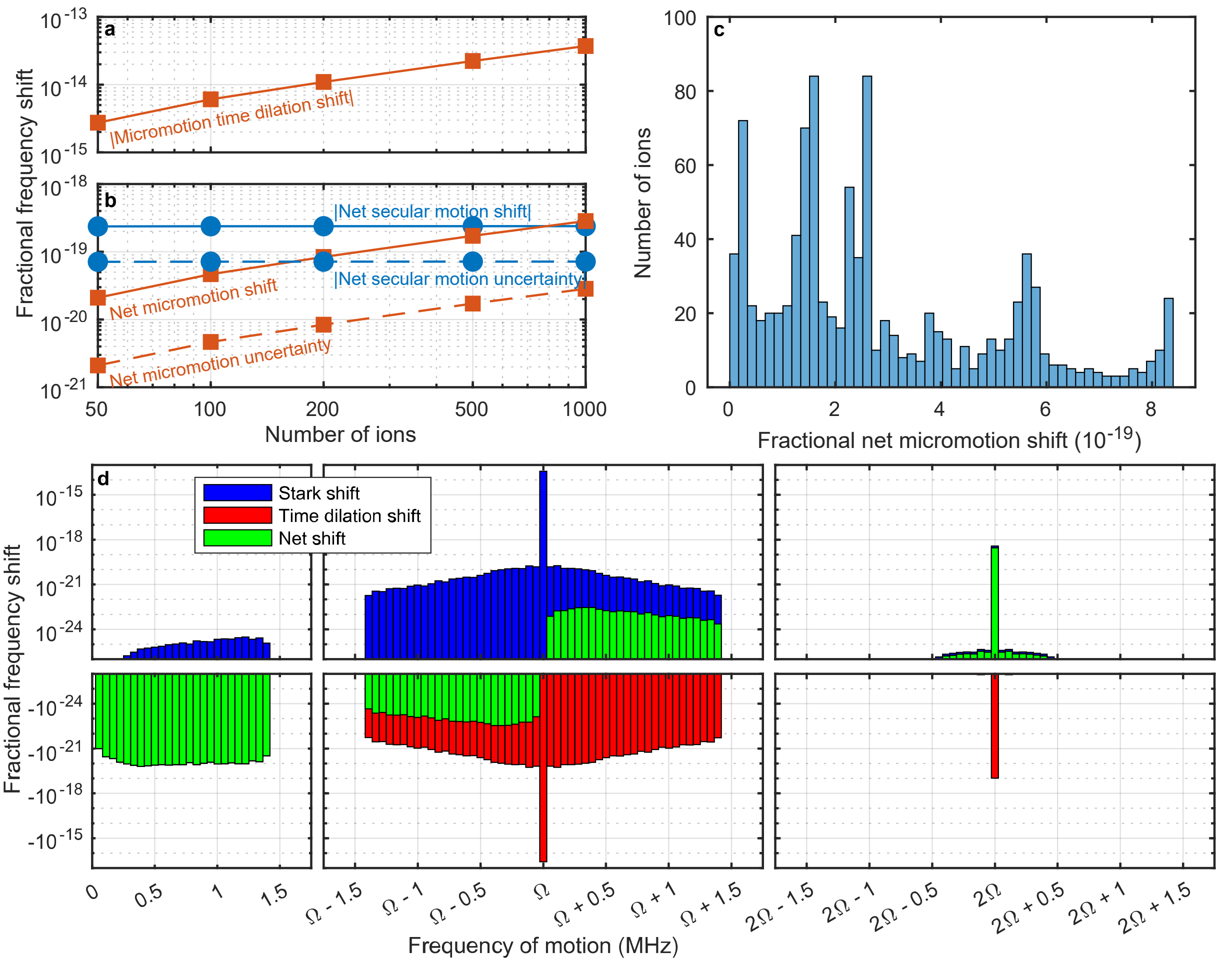

FIG. 3. Systematic frequency shifts due to ion motion. (a) Absolute value of the time-dilation shift due to micromotion, averaged over all of the ions, as a function of the number of ions in the trap. As the number of ions increases, some of the ions are located further away from the trap axis where micromotion is minimized, leading to an increase in the average micromotion time-dilation shift. (b) Absolute value of the net micromotion and secular motion shifts, averaged over all of the ions, as a function of the number of ions in the trap. The net shift is defined as the sum of the negative time-dilation shift and the positive Stark shift due to the electric field of the ion trap. Also shown are estimated uncertainties in how well these shifts can be characterized. (c) Histogram showing the number of ions out of a 1000 ion Coulomb crystal with a net micromotion shift within each bin. Each ion is located at a different position within the trap and thus experiences different micromotion and Stark shifts, but the inhomogeneous broadening associated with these shifts is below 10^{-18} fractionally and should not impact spectroscopic coherence within the foreseeable future. (d) Histogram of motional frequency shifts as a function of the frequency of the ion motion, for a 1000 ion Coulomb crystal. All 3000 secular modes have frequencies below 1.5 MHz. For motion at these frequencies the magnitude of the time-dilation shift is much larger than the Stark shift due to trapping fields and the green bars indicating the net shift are covering up the red bars indicating the time-dilation shift. At the magic trap drive frequency $\Omega_m/(2\pi) \approx 225$ MHz, the micromotion time-dilation shift is exactly canceled by the corresponding trap Stark shift, but at secular motion sidebands of the trap drive frequency this cancellation is imperfect. At the second harmonic of the trap drive frequency, the Stark shift is much larger than the time-dilation shift and dominates the net shift.

the clock transition under these conditions. The contrast is limited to 79 % due to the inhomogeneous reduction of the Rabi frequency by the Debye-Waller effect, and a broad band of overlapping motional sideband transitions surrounds the carrier transition which is at zero detuning. The lowest frequency motional sideband transitions are above 14 kHz for any of the generated crystal configurations, and should not lead to significant line-pulling due to off-resonant excitation for probe times longer than about 10 ms.

The trap parameters can be optimized to minimize the net micromotion shift, minimize the size of the ion crystal and thus inhomogenous broadening due to magnetic field gradients as well as required laser beam diameters, maximize the lowest secular frequency, maximize the spectroscopy contrast, or for other goals. Furthermore, the

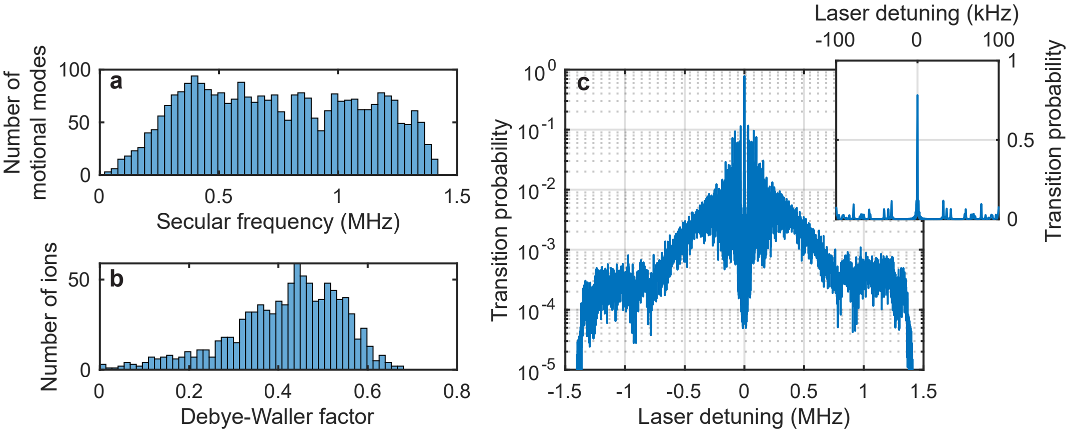

FIG. 4. Effects of ion motion in a 1000 ion Coulomb crystal at a motional temperature of 120 μK on spectroscopy of the clock transition. (a) Histogram showing the number of collective motional normal modes binned by the motional mode frequency, which ranges from a minimum of 32 kHz up to a maximum of 1.419 MHz. (b) Histogram showing the number of ions binned by the Debye-Waller factor due to secular motion, which relates the Rabi frequency for driving the clock transition in an ion at rest with the Rabi frequency for an ion undergoing secular motion. (c) Calculated spectrum of the clock transition probed using Rabi spectroscopy with a probe duration of 1 ms and a laser intensity that maximizes the on-resonance transition probability, averaged over all of the ions. The inset is an enlargement of the region near the atomic transition frequency, showing the carrier at zero detuning and a few discrete motional sidebands. For larger detunings shown in the main plot, the motional sidebands overlap in frequency to form broad bands.

number of ions can be selected to balance systematic shifts and inhomogeneous broadening that increase with the number of ions versus the QPN stability limit that decreases with increasing numbers of ions. Figure 5 shows a limited subset of this trade space. The lowest normal mode secular frequency for trap parameters such that the single-ion secular frequencies are 1.15 MHz, 0.85 MHz, and 0.10 MHz decreases as the number of ions increases, reaching a mean value of 32 kHz for 1000 ions with a distribution spanning from 15 kHz to 56 kHz for different crystal configurations. For single-ion secular frequencies that are too low or too high relative to the radial single-ion secular frequencies, the spectroscopy contrast is reduced. Single-ion secular frequencies of 1.15 MHz, 0.85 MHz, and 0.10 MHz represent a tradeoff of all of the aforementioned optimization goals.

DISCUSSION

Performance of a 1000 ion Sn^{2+} clock. We estimate that the total systematic uncertainty of a 1000 ion Sn^{2+} clock operated under the conditions specified above could be suppressed to the 9.0×10^{-20} level or beyond (see Tab. III). The largest shift at 15 G magnetic field is the quadratic Zeeman shift at -3.7×10^{-15}, but this can be controlled and characterized very well. Performing a measurement of the quadratic Zeeman shift at 100 G field with a fractional frequency uncertainty of 10^{-18} would determine the atomic coefficient such that the corresponding uncertainty of the shift at 15 G is $10^{-18}/(100\ \text{G}/15\ \text{G}) = 2.3 \times 10^{-20}$. Characterization of the magnetic field with 10 μG uncertainty would reduce the associated uncertainty of the quadratic Zeeman shift to 4.9×10^{-21}. This could be accomplished in-situ by measuring the splitting of the extreme Zeeman sublevels of the metastable ${}^3P_2$ state with 84 Hz uncertainty, via two-photon Raman excitation from the ground state using lasers detuned from the 181 nm ${}^1S_0 \leftrightarrow {}^3P_1$ and 2481 nm ${}^3P_1 \leftrightarrow {}^3P_2$ transitions. The next-largest shift is the probe laser Stark shift for single-photon spectroscopy, but the uncertainty of this shift can be suppressed to a negligible level using hyper-Ramsey [26] or auto-balanced Ramsey [27] interrogation protocols. The 5.2×10^{-18} Stark shift due to blackbody radiation (BBR) at 300 K can be characterized with an uncertainty of 3.4×10^{-20} by measuring the static differential polarizability following Dub *et al.* [25] and the dynamic correction using a few far-IR lasers [18, 33], and characterizing the temperature of the BBR with an uncertainty of 500 mK [34]. Alternatively, the BBR shift can be suppressed to a negligible level by cooling the ion trap and thus the BBR to cryogenic temperatures [35–37]. The electric quadrupole shift is negligible because the total electronic angular momentum of both clock states is zero [38]. The largest uncertainty in our estimate is due to secular motion time dilation, and it may be possible to reduce this by characterizing the motional temperature better than our conservative assumption of 30 %.

The stability of the clock is fundamentally limited by QPN at $4.4 \times 10^{-18}/\tau^{1/2}$ where τ is the measurement

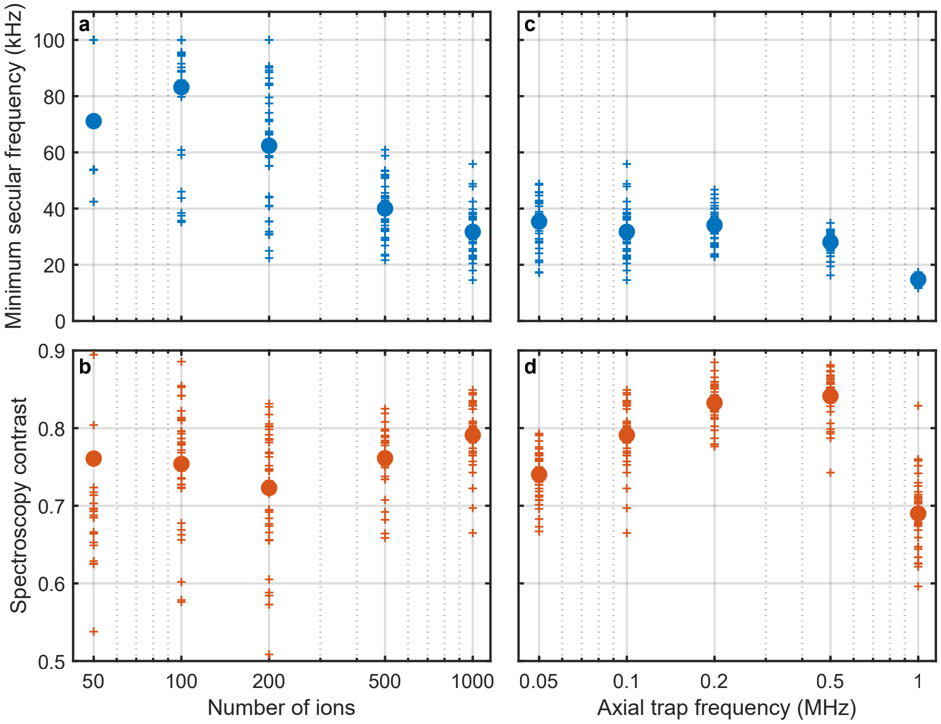

FIG. 5. Minimum secular frequency and maximum possible spectroscopic contrast at a motional temperature of 120 μK for different Coulomb crystal configurations. (a) Minimum secular frequency and (b) average spectroscopy contrast as a function of the number of trapped ions for trap parameters such that the secular frequencies of a single Sn^{2+} ion are 1.15 MHz, 0.85 MHz, and 0.10 MHz. For Coulomb crystals containing many ions, there are multiple local minima of the total Coulomb energy corresponding to distinct stable geometric crystal configurations. For each number of ions, 36 configurations were generated by numerically integrating the equations of motion including a damping term which qualitatively represents laser cooling starting from randomized initial ion positions. Each of the configurations that were generated is plotted as a small cross, while the average of all of the generated configurations is plotted as a large circle. As the number of ions increases, the minimum secular frequency decreases but the spectroscopy contrast remains relatively constant. Off-resonant driving of low-frequency motional sideband transitions can lead to detrimental line pulling of the clock transition carrier. (c) Minimum secular frequency and (d) average spectroscopy contrast as a function of the single-ion axial secular frequency for 1000 ions and single-ion radial secular frequencies 1.15 MHz and 0.85 MHz. As the single-ion axial secular frequency nears degeneracy with the single-ion radial secular frequencies, the minimum secular frequency and the average spectroscopy constrast go down.

duration in seconds, assuming a conservative 1 s probe duration and 80 % duty cycle. This is nearly two orders of magnitude better than the best clock-comparison stability achieved with an ion clock [6, 39] and one order of magnitude better than the best stability comparison of independent lattice clocks [40]. At this level, it is possible to perform frequency measurements with a total uncertainty of 10^{-19} in under three hours, measure the time-dependent gravitational effects of solid-Earth tides with high signal-to-noise ratio [41], and search for ultralight bosonic dark matter (DM) candidates over a broad range of particle masses [42].

It may be possible to achieve yet higher performance than discussed here by co-trapping a second ion species such as Sr^{+} together with Sn^{2+} in the trap. Due to the higher mass-to-charge ratio of Sr^{+}, the Sr^{+} ions would reside on the outside edge of the crystal, pushing the Sn^{2+} ions towards the trap axis where the micromotion shift is smaller. Sr^{+} could be used to perform sympathetic laser cooling of the two-species Coulomb crystal both with a higher cooling rate on the 422 nm $S_{1/2} \leftrightarrow P_{1/2}$ transition before clock interrogation and to a lower tem-

TABLE III. Fractional systematic shifts and estimated uncertainties of a 1000 ion Sn^{2+} clock, operating at a magnetic field of 15 G in a room temperature ion trap with a blackbody radiation temperature of 300.0(5) K.

Effect	Shift (10^{-20})	Uncertainty (10^{-20})
Secular motion	-24	7.2
Blackbody radiation shift	515	3.4
Micromotion	28	2.8
Quadratic Zeeman shift	-366550	2.3
Probe laser Stark shift	19753	2.0
Total	-346278	9.0

perature continuously during clock interrogation using the 674 nm $S_{1/2} \leftrightarrow D_{5/2}$ transition. The magnetic field could be characterized by measuring the splitting of the Zeeman sublevels of the $D_{5/2}$ state. Another possibility to consider is that a multi-pole linear Paul trap could be used [43–45]. Ions near the trap axis in multi-pole traps experience less micromotion than in conventional quadrupole traps, and with co-trapped Sr^+ pushing the Sn^{2+} towards the trap axis it may be possible to dramatically suppress the micromotion shift and corresponding uncertainty. Using these techniques, it may also be possible to increase the ion number to much larger than 1000 and achieve even higher precision while maintaining sub-10^{-19} inaccuracy.

Sensitivity to beyond Standard Model physics. Precision measurements of frequency differences between different isotopes of two or more atomic transitions [46–48] can be used to search for hypothetical new bosons in the intermediate mass range that mediate interactions between quarks and leptons [49, 50]. Such isotope shift data are analysed using a King plot, where mass-scaled frequency shifts of two optical transitions are plotted against each other for a series of isotopes [51]. The leading standard model contributions to the isotope shift (IS), mass and field shifts, give a linear relationship between two electronic transitions with respect to different IS measurements. New spin-independent interactions will break this relation, and thus can be probed by looking for a non-linearity of the King plot [49, 50]. Data for at least four even isotopes are needed to detect the non-linearity. In addition to the $^1S_0 \leftrightarrow ^3P_0$ clock transition that we focus on in this article, Sn^{2+} also has a $^1S_0 \leftrightarrow ^3P_2$ clock transition that is capable of supporting very high accuracy and precision spectroscopy.

Higher-order standard model contributions could break the linearity of the King plot as well [50], and must either be calculated with high accuracy [52], which is very difficult, or eliminated together with uncertainties of the isotope mass differences using more transitions and/or isotopes in a generalized analysis [53, 54]. In particular, nuclear structure properties such as the quadrupole deformation and higher order nuclear moments can cause a non-linearity in the King plot. Sn^{2+} is unique in that it is the element with the greatest number of stable isotopes: in particular there are 7 stable isotopes with zero nuclear spin ($^{112}Sn^{2+}$, $^{114}Sn^{2+}$, $^{116}Sn^{2+}$, $^{118}Sn^{2+}$, $^{120}Sn^{2+}$, $^{122}Sn^{2+}$, and $^{124}Sn^{2+}$), an additional nuclear-spin-zero isotope with a lifetime of 230,000 years ($^{126}Sn^{2+}$), and 10 more nuclear-spin-zero isotopes with a lifetime greater than 1 s that could be studied at rare isotope facilities. Additional transitions in other charge states could also be measured: the 583 nm $^3P_0 \leftrightarrow ^1S_0$ intercombination transition in Sn, the sub-Hz linewidth 2352 nm $^2P_{1/2} \leftrightarrow ^1P_{3/2}$ magnetic dipole transition in Sn^+, and perhaps more. Therefore, Sn^{2+} is particularly well-suited for new physics searches with the generalized analysis [53, 54] where nuclear structure uncertainties are removed by using data from more isotopes in order to separate higher order Standard Model effects in the nucleus and the signal due to a hypothetical new boson [47, 48]. This is especially important in light of recent experiments in neutral Yb and Yb^+ that detected the non-linear effects that may be caused by higher-order contributions within the standard model [46–48].

Hypothesized ultralight bosonic DM candidates would behave as a highly-coherent classical field that oscillates at the Compton frequency corresponding to the DM particle mass $f_\phi = m_\phi c^2/h$, where m_ϕ is the mass, c is the speed of light, and h is Planck's constant. This field is predicted to couple to atomic transition frequencies and would be detectable by measuring the ratio of two atomic transition frequencies or the difference between an atomic transition frequency and a Fabry-Perot resonator that have different sensitivities to the DM coupling [42]. Many ion clocks can be sensitive to a broad range of DM particle masses due to their high stability at short measurement durations discussed above. Although in standard clock operation the upper limit to the measurement bandwidth and thus DM particle mass is given by the reciprocal of the probe duration, dynamical decoupling can be used to extend sensitivity up to much higher frequencies [42]. High stability of Sn^{2+} clock makes it also competitive with lattice clocks for proposed space tests of general relativity [55].

Summary and outlook. We have proposed Coulomb crystal optical atomic clocks based on many Sn^{2+} ions confined in a linear RF Paul trap as a candidate for a new metrological platform that offers the possibility of precision better than any present-day optical lattice clock and accuracy better than any present-day single-ion clock. Sn^{2+} is unique among candidates for Coulomb-crystal clocks because it has a highly-forbidden intercombination clock transition between two states with zero electronic angular momentum, a spin-zero nucleus that eliminates nonscalar perturbations, a negative differential polarizability that enables cancellation of the micromotion time-dilation shift by the associated Stark shift, and an accessible direct laser cooling and readout transition. Beyond applications in timekeeping, this platform has the potential to find applications in relativistic geodesy, searches for physics beyond the Standard Model, and more.

METHODS

Quadrupole moment. The quadrupole moment Θ of an atomic state $|J\rangle$ is given by

$$\begin{aligned}\Theta &= 2\,\langle J, M_J = J|Q_0|J, M_J = J\rangle \\ &= 2\sqrt{\frac{J(2J-1)}{(2J+3)(J+1)(2J+1)}}\langle J||Q||J\rangle, \qquad (3)\end{aligned}$$

where $\langle J||Q||J\rangle$ is the reduced matrix element of the electric quadrupole operator.

For the $5s5p\,^3P_2$ state, we find

$$\langle ^3P_2||Q||^3P_2\rangle \approx -6.9\, ea_0^2 \tag{4}$$

and

$$\Theta(^3P_2) \approx -3.3\, ea_0^2. \tag{5}$$

Zeeman shift. Since we consider the ion with $J = I = 0$, there is no linear Zeeman shift. The second-order Zeeman shift, ΔE, is given by [56]

$$\begin{aligned}\Delta E &\equiv \Delta E^{(1)} + \Delta E^{(2)} \\ &\approx -\frac{1}{2}\alpha^{\rm M1}B^2 + \frac{\mu_0^2\, m}{2\hbar^2}\sum_{i=1}^{Z}\langle 0\,|(\mathbf{B}\times\mathbf{r}_i)^2|\,0\rangle,\end{aligned} \tag{6}$$

where $\alpha^{\rm M1}$ is the magnetic-dipole static polarizability, μ_0 is the Bohr magneton, m is the electron mass, and $\mathbf{r}_i$ is the position vector of the ith electron. For a state $|J=0\rangle$, the polarizability can be written as

$$\alpha^{\rm M1} = \frac{2}{3}\sum_n \frac{|\langle n||\mu||J=0\rangle|^2}{E_n - E_0}. \tag{7}$$

To estimate the shift for the clock transition due to this term, we note that the $\alpha^{M1}(^1S_0)$ polarizability is negligibly small compared to $\alpha^{M1}(^3P_0)$, so we have

$$\Delta\nu^{(1)} \equiv \frac{\Delta E(^3P_0) - \Delta E(^1S_0)}{h} \approx \Delta E(^3P_0)/h.$$

For an estimate of $\alpha^{M1}(^3P_0)$, we take into account that the main contribution to this polarizability comes from the intermediate state $5s5p\ ^3P_1$. Then, from Eq. (7), we obtain

$$\alpha^{\rm M1}(^3P_0) \approx \frac{2}{3}\frac{\langle ^3P_1||\mu||^3P_0\rangle^2}{E_{^3P_1} - E_{^3P_0}}. \tag{8}$$

We found the matrix element $|\langle ^3P_1||\mu||^3P_0\rangle|$ to be $1.4064\,\mu_0$ and $1.4053\,\mu_0$ in the CI+all-order and CI+MBPT approximations, respectively. These values differ by 0.07%. According to our calculation, the next (after $^3P_1$) intermediate state in Eq. (7), $^1P_1$, contributes to $\alpha^{\rm M1}(^3P_0)$ at the level of 0.06% compared to the contribution of the $^3P_1$ state. Conservatively, estimating the contribution of all other intermediate states as $2\times 0.06\%$, we arrive at the uncertainty of $\Delta\nu^{(1)}$ at the level of 0.2%.

Using it and the experimental value of the energy difference $E_{^3P_1} - E_{^3P_0} \approx 1648$ cm^{-1}, we arrive at

$$\Delta\nu^{(1)} \approx -2.616(5)\ \frac{\rm MHz}{\rm T^2}\, B^2,$$

where the magnetic field B is expressed in T.

One can show [56] that the contribution of the second term in Eq. (6) to the second-order Zeeman shift of the clock transition can be written as

$$\begin{aligned}\Delta\nu^{(2)} &\equiv \frac{(2\pi\mu_0)^2 m}{3h^3}B^2 \\ &\times \sum_{i=1}^{Z}\left\{\langle ^3P_0|r_i^2|\,^3P_0\rangle - \langle ^1S_0|r_i^2|\,^1S_0\rangle\right\},\end{aligned} \tag{9}$$

where the matrix elements are expressed in a_0^2.

The calculation, carried out in the framework of our approach, leads to

$$\sum_{i=1}^{Z}\left\{\langle ^3P_0|r_i^2|\,^3P_0\rangle - \langle ^1S_0|r_i^2|\,^1S_0\rangle\right\} \approx 1.7\, a_0^2. \tag{10}$$

To check this result, we made another calculation, reconstructing the basis set and using the pure CI method, where all 48 electrons were placed in the valence field, and several of the most important configurations were included into consideration. We obtained the same value $1.7\, a_0^2$.

Using this result, we find

$$\Delta\nu^{(2)} \approx 0.017(2)\ \frac{\rm MHz}{\rm T^2}\, B^2.$$

We estimate the uncertainty of this term at the level of 10%.

Finally, we find the quadratic Zeeman shift as

$$|\Delta\nu| = |\Delta\nu^{(1)} + \Delta\nu^{(2)}| \approx 2.598(5)\ \frac{\rm MHz}{\rm T^2}\, B^2. \tag{11}$$

Rabi frequency. The Rabi frequency of the one-photon $^1S_0 -\ ^3P_0$ transition is determined as

$$\Omega = \langle \widetilde{^3P_0}|\mathbf{d}\boldsymbol{\mathcal{E}}|\,^1S_0\rangle/\hbar, \tag{12}$$

where $\boldsymbol{\mathcal{E}}$ is the electric field of the laser wave and we designate

$$|\widetilde{^3P_0}\rangle \equiv |^3P_0\rangle + \sum_n \frac{|n\rangle\langle n|\boldsymbol{\mu}\mathbf{B}|^3P_0\rangle}{E_{^3P_0} - E_n}. \tag{13}$$

Substituting Eq. (13) to Eq. (12), we arrive after simple transformation at

$$\hbar\Omega = \frac{(\mathbf{B}\boldsymbol{\mathcal{E}})}{3}\sum_n \frac{\langle ^3P_0||\mu||n\rangle\langle n||d||\,^1S_0\rangle}{E_n - E_{^3P_0}}. \tag{14}$$

Leaving (for an estimate) in the sum of Eq. (14) only two intermediate states, $5s5p\ ^3P_1$ and $5s5p\ ^1P_1$, and using our calculated values $|\langle ^3P_0||d||\,^3P_1\rangle| \approx 1.406\,\mu_0$ and $|\langle ^3P_1||d||\,^1S_0\rangle| \approx 0.249\, ea_0$, we find

$$|\Omega|/(2\pi) \approx 34\ \frac{\rm Hz}{\rm T\sqrt{mW/cm^2}}\, \sqrt{I}B\cos\theta, \tag{15}$$

where I is the laser intensity and θ is the angle between $\mathbf{B}$ and $\boldsymbol{\mathcal{E}}$.

The clock transition can also be driven as the two-photon $E1+M1$ transition. The respective formalism was developed in Ref. [19]. The $E1+M1$ Rabi frequency, Ω_2, is given by

$$\Omega_2 = \frac{4\pi}{3\varepsilon_0 hc^2}\sqrt{I_1 I_2}\,\Lambda, \tag{16}$$

where Λ can be written in terms of dominant contributions as

$$\Lambda \approx \left| \sum_{n={}^3P_1,{}^1P_1} \frac{\langle {}^3P_0||\mu||n\rangle\langle n||d||\,{}^1S_0\rangle}{E_n - E_{{}^3P_0}/2} \right| \tag{17}$$

and I_1 and I_2 are the intensities of two probe laser waves. Using the experimental energies and the values of the MEs given in Table I, we find

$$\frac{\Omega_2}{2\pi} \approx 0.27 \frac{\text{Hz}}{\text{kW/cm}^2}\sqrt{I_1 I_2}. \tag{18}$$

---

* david.leibrandt@nist.gov

[1] A. D. Ludlow, M. M. Boyd, J. Ye, E. Peik, and P. O. Schmidt, Optical atomic clocks, Rev. Mod. Phys. **87**, 637 (2015).

[2] W. F. Mcgrew, X. Zhang, R. J. Fasano, S. A. Schffer, K. Beloy, D. Nicolodi, R. C. Brown, N. Hinkley, G. Milani, M. Schioppo, T. H. Yoon, and A. D. Ludlow, Atomic clock performance enabling geodesy below the centimetre level, Nature **564**, 87 (2018).

[3] M. S. Safronova, D. Budker, D. DeMille, D. F. J. Kimball, A. Derevianko, and C. W. Clark, Search for new physics with atoms and molecules, Rev. Mod. Phys. **90**, 025008 (2018).

[4] D. B. Hume and D. R. Leibrandt, Probing beyond the laser coherence time in optical clock comparisons, Phys. Rev. A **93**, 032138 (2016).

[5] S. Drscher, A. Al-Masoudi, M. Bober, R. Schwarz, R. Hobson, U. Sterr, and C. Lisdat, Dynamical decoupling of laser phase noise in compound atomic clocks, Commun. Phys. **3**, 185 (2020).

[6] M. E. Kim, W. F. McGrew, N. V. Nardelli, E. R. Clements, Y. S. Hassan, X. Zhang, J. Valencia, H. Leopardi, D. B. Hume, T. M. Fortier, A. D. Ludlow, and D. R. Leibrandt, Optical coherence between atomic species at the second scale: improved clock comparisons via differential spectroscopy, arXiv:2109.09540 (2021).

[7] J. Keller, T. Burgermeister, D. Kalincev, A. Didier, A. P. Kulosa, T. Nordmann, J. Kiethe, and T. E. Mehlstubler, Controlling systematic frequency uncertainties at the 10^{-19} level in linear coulomb crystals, Phys. Rev. A **99**, 013405 (2019).

[8] A. W. Young, W. J. Eckner, W. R. Milner, D. Kedar, M. A. Norcia, E. Oelker, N. Schine, J. Ye, and A. M. Kaufman, Half-minute-scale atomic coherence and high relative stability in a tweezer clock, Nature **588**, 408 (2020).

[9] S. L. Campbell, R. B. Hutson, G. E. Marti, A. Goban, N. D. Oppong, R. L. McNally, L. Sonderhouse, J. M. Robinson, W. Zhang, B. J. Bloom, and J. Ye, A fermi-degenerate three-dimensional optical lattice clock, Science **358**, 90 (2017).

[10] M. Drewsen, C. Brodersen, L. Hornekr, J. S. Hangst, and J. P. Schifffer, Large ion crystals in a linear Paul trap, Phys. Rev. Lett. **81**, 2878 (1998).

[11] T. Schtz, U. Schramm, and D. Habs, Crystalline ion beams, Nature **412**, 717 (2001).

[12] N. Kjrgaard and M. Drewsen, Observation of a structural transition for Coulomb crystals in a linear Paul trap, Phys. Rev. Lett. **91**, 095002 (2003).

[13] P. F. Herskind, A. Dantan, J. P. Marler, M. Albert, and M. Drewsen, Realization of collective strong coupling with ion Coulomb crystals in an optical cavity, Nature Phys. **5**, 494 (2009).

[14] M. Albert, A. Dantan, and M. Drewsen, Cavity electromagnetically induced transparency and all-optical switching using ion Coulomb crystals, Nature Photon. **5**, 633 (2011).

[15] Y.-K. Wu, Z.-D. Liu, W.-D. Zhao, and L.-M. Duan, High-fidelity entangling gates in a three-dimensional ion crystal under micromotion, Phys. Rev. A **103**, 022419 (2021).

[16] D. J. Berkeland, J. D. Miller, J. C. Bergquist, W. M. Itano, and D. J. Wineland, Minimization of ion micromotion in a Paul trap, J. App. Phys. **83**, 5025 (1998).

[17] K. Arnold, E. Hajiyev, E. Paez, C. H. Lee, and M. D. Barrett, Prospects for atomic clocks based on large ion crystals, Phys. Rev. A **92**, 032108 (2015).

[18] K. J. Arnold, R. Kaequam, A. Roy, T. R. Tan, and M. D. Barrett, Blackbody radiation shift assessment for a lutetium ion clock, Nature Communications **9**, 1650 (2018).

[19] K. Beloy, Prospects of a Pb^{2+} ion clock, Phys. Rev. Lett. **127**, 013201 (2021).

[20] P. O. Schmidt, T. Rosenband, C. Langer, W. M. Itano, J. C. Bergquist, and D. J. Wineland, Spectroscopy using quantum logic, Science **309**, 749 (2005).

[21] M. S. Safronova, M. G. Kozlov, W. R. Johnson, and D. Jiang, Development of a configuration-interaction plus all-order method for atomic calculations, Phys. Rev. A **80**, 012516 (2009).

[22] V. A. Dzuba, V. V. Flambaum, and M. G. Kozlov, Combination of the many-body perturbation theory with the configuration-interaction method, Phys. Rev. A **54**, 3948 (1996).

[23] A. Heinz, A. J. Park, N. Šantić, J. Trautmann, S. G. Porsev, M. S. Safronova, I. Bloch, and S. Blatt, State-Dependent Optical Lattices for the Strontium Optical Qubit, Phys. Rev. Lett. **124**, 203201 (2020), arXiv:1912.10350 [physics.atom-ph].

[24] Yu. Ralchenko, A. Kramida, J. Reader, and the NIST ASD Team (2011). NIST Atomic Spectra Database (version 4.1). Available at http://physics.nist.gov/asd. National Institute of Standards and Technology, Gaithersburg, MD.

[25] P. Dub, A. A. Madej, M. Tibbo, and J. E. Bernard, High-accuracy measurement of the differential scalar polarizability of a $^{88}\text{Sr}^+$ clock using the time-dilation effect, Phys. Rev. Lett. **112**, 173002 (2014).

[26] N. Huntemann, B. Lipphardt, M. Okhapkin, C. Tamm, E. Peik, A. V. Taichenachev, and V. I. Yudin, Generalized Ramsey excitation scheme with suppressed light

shift, Phys. Rev. Lett. **109**, 213002 (2012).

[27] C. Sanner, N. Huntemann, R. Lange, C. Tamm, and E. Peik, Autobalanced Ramsey spectroscopy, Phys. Rev. Lett. **120**, 053602 (2018).

[28] R. W. Hasse, A semiempirical mass formula for spherical Coulomb crystals, J. Phys. B: At. Mol. Opt. Phys. **36**, 1011 (2003).

[29] A. Mortensen, E. Nielsen, T. Matthey, and M. Drewsen, Observation of three-dimensional long-range order in small ion Coulomb crystals in an rf trap, Phys. Rev. Lett. **96**, 103001 (2006).

[30] D. F. V. James, Quantum dynamics of cold trapped ions with application to quantum computation, Appl. Phys. B **66**, 181 (1998).

[31] D. J. Wineland, C. Monroe, W. M. Itano, D. Leibfried, B. E. King, and D. M. Meekhof, Experimental issues in coherent quantum-state manipulation of trapped atomic ions, J. Res. Natl. Inst. Stand. Technol. **103**, 259 (1998).

[32] J.-S. Chen, S. M. Brewer, C. W. Chou, D. J. Wineland, D. R. Leibrandt, and D. B. Hume, Sympathetic ground state cooling and time-dilation shifts in an $^{27}\mathrm{Al}^{+}$ optical clock, Phys. Rev. Lett. **118**, 053002 (2017).

[33] N. Huntemann, C. Sanner, B. Lipphardt, C. Tamm, and E. Peik, Single-ion atomic clock with 3×10^{-18} systematic uncertainty, Phys. Rev. Lett. **116**, 063001 (2016).

[34] M. Doleal, P. Balling, P. B. R. Nisbet-Jones, S. A. King, J. M. Jones, H. A. Klein, P. Gill, T. Lindvall, A. E. Wallin, M. Merimaa, C. Tamm, C. Sanner, N. Huntemann, N. Scharnhorst, I. D. Leroux, P. O. Schmidt, T. Burgermeister, T. E. Mehlstubler, and E. Peik, Analysis of thermal radiation in ion traps for optical frequency standards, Metrologia **52**, 842 (2015).

[35] W. H. Oskay, S. A. Diddams, E. A. Donley, T. M. Fortier, T. P. Heavner, L. Hollberg, W. M. Itano, S. R. Jefferts, M. J. Delaney, K. Kim, F. Levi, T. E. Parker, and J. C. Bergquist, Single-atom optical clock with high accuracy, Phys. Rev. Lett. **97**, 020801 (2006).

[36] I. Ushijima, M. Takamoto, M. Das, T. Ohkubo, and H. Katori, Cryogenic optical lattice clocks, Nature Photon. **9**, 185 (2015).

[37] Y. Huang, B. Zhang, M. Zeng, Y. Hao, Z. Ma, H. Zhang, H. Guan, Z. Chen, M. Wang, and K. Gao, Liquid-nitrogen-cooled Ca^{+} optical clock with systematic uncertainty of 3×10^{-18}, Phys. Rev. Applied **17**, 034041 (2022).

[38] K. Beloy, D. R. Leibrandt, and W. M. Itano, Hyperfine-mediated electric quadrupole shifts in Al^{+} and In^{+} ion clocks, Phys. Rev. A **95**, 043405 (2017).

[39] E. R. Clements, M. E. Kim, K. Cui, A. M. Hankin, S. M. Brewer, J. Valencia, J.-S. Chen, C.-W. Chou, D. R. Leibrandt, and D. B. Hume, Lifetime-limited interrogation of two independent $^{27}\mathrm{Al}^{+}$ clocks using correlation spectroscopy, Phys. Rev. Lett. **125**, 243602 (2020).

[40] E. Oelker, R. B. Hutson, C. J. Kennedy, L. Sonderhouse, T. Bothwell, A. Goban, D. Kedar, C. Sanner, J. M. Robinson, G. E. Marti, D. G. Matei, T. Legero, M. Giunta, R. Holzwarth, F. Riehle, U. Sterr, and J. Ye, Demonstration of 4.8×10^{17} stability at 1 s for two independent optical clocks, Nature Photon. **13**, 714 (2019).

[41] T. E. Mehlstubler, G. Grosche, C. Lisdat, P. O. Schmidt, and H. Denker, Atomic clocks for geodesy, Rep. Prog. Phys. **81**, 064401 (2018).

[42] D. Antypas *et al.*, New horizons: Scalar and vector ultralight dark matter, arXiv:2203.14915 (2022).

[43] J. D. Prestage, R. L. Tjoelker, and L. Maleki, Higher pole linear traps for atomic clock applications, in *Proc. 1999 Joint European Frequency and Time Forum and IEEE International Frequency Control Symposium* (IEEE, 1999) p. 121.

[44] O. Asvany, S. Brnken, L. Kluge, and S. Schlemmer, Coltrap: a 22-pole ion trapping machine for spectroscopy at 4 K, Appl. Phys. B **114**, 203 (2013).

[45] E. A. Burt, J. D. Prestage, R. L. Tjoelker, D. G. Enzer, D. Kuang, D. W. Murphy, D. E. Robison, J. M. Seubert, R. T. Wang, and T. A. Ely, Demonstration of a trapped-ion atomic clock in space, Nature **595**, 43 (2021).

[46] I. Counts, J. Hur, D. P. L. A. Craik, H. Jeon, C. Leung, J. C. Berengut, A. Geddes, A. Kawasaki, W. Jhe, and V. Vuleti, Evidence for nonlinear isotope shift in Yb^{+} search for new boson, Phys. Rev. Lett. **125**, 123002 (2020).

[47] J. Hur, D. P. A. Craik, I. Counts, E. Knyazev, L. Caldwell, C. Leung, S. Pandey, J. C. Berengut, A. Geddes, W. Nazarewicz, P.-G. Reinhard, A. Kawasaki, H. J. amd Wonho Jhe, and V. Vuleti, Evidence of two-source King plot nonlinearity in spectroscopic search for new boson, Phys. Rev. Lett. **128**, 163201 (2022).

[48] N. Figueroa, J. Berengut, V. Dzuba, V. Flambaum, D. Budker, and D. Antypas, Precision determination of isotope shifts in ytterbium and implications for new physics, Phys. Rev. Lett. **128**, 073001 (2022).

[49] C. Delaunay, R. Ozeri, G. Perez, and Y. Soreq, Probing atomic higgs-like forces at the precision frontier, Phys. Rev. D **96**, 093001 (2017).

[50] J. C. Berengut, D. Budker, C. Delaunay, V. V. Flambaum, C. Frugiuele, E. Fuchs, C. Grojean, R. Harnik, R. Ozeri, G. Perez, and Y. Soreq, Probing new long-range interactions by isotope shift spectroscopy, Phys. Rev. Lett. **120**, 091801 (2018).

[51] W. H. King, Comments on the article "peculiarities of the isotope shift in the samarium spectrum", J. Opt. Soc. Am. **53**, 638 (1963).

[52] V. A. Yerokhin, R. A. Müller, A. Surzhykov, P. Micke, and P. O. Schmidt, Nonlinear isotope-shift effects in Be-like, B-like, and C-like argon, Phys. Rev. A **101**, 012502 (2020).

[53] K. Mikami, M. Tanaka, and Y. Yamamoto, Probing new intra-atomic force with isotope shifts, Eur. Phys. J. C **77**, 896 (2017).

[54] J. C. Berengut, C. Delaunay, A. Geddes, and Y. Soreq, Generalized king linearity and new physics searches with isotope shifts, Physical Review Research **2**, 10.1103/physrevresearch.2.043444 (2020).

[55] A. Derevianko, K. Gibble, L. Hollberg, N. R. Newbury, C. Oates, M. S. Safronova, L. C. Sinclair, and N. Yu, Fundamental physics with a state-of-the-art optical clock in space (2021).

[56] S. G. Porsev and M. S. Safronova, Calculation of higher-order corrections to the light shift of the $5s^2\,{}^1S_0-5s5p\,{}^3P_0$ clock transition in Cd, Phys. Rev. A **102**, 012811 (2020).

ACKNOWLEDGEMENTS

This work was supported by the National Institute of Standards and Technology, the Defense Advanced Research Projects Agency (Atomic-Photonic Integration Program), the National Science Foundation Q-SEnSE Quantum Leap Challenge Institute (Grant Number 2016244), the National Science Foundation (Grant Number PHY-2012068), the Office of Naval Research (Grant Numbers N00014-18-1-2634 and N00014-20-1-2513), and the European Research Council (ERC) under the European Unions Horizon 2020 research and innovation program (Grant Number 856415). This research was supported in part through the use of University of Delaware HPC Caviness and DARWIN computing systems: DARWIN - A Resource for Computational and Data-intensive Research at the University of Delaware and in the Delaware Region, Rudolf Eigenmann, Benjamin E. Bagozzi, Arthi Jayaraman, William Totten, and Cathy H. Wu, University of Delaware, 2021, URL: https://udspace.udel.edu/handle/19716/29071.

The views, opinions, and/or findings expressed are those of the authors and should not be interpreted as representing the official views or policies of the Department of Defense or the U.S. Government.

AUTHOR CONTRIBUTIONS

D.R.L. conceived the idea. S.G.P., C.C., and M.S.S. performed the calculations of Sn^{2+} atomic properties. D.R.L. performed the calculations of ion motion in Coulomb crystals. All authors discussed the results and implications and contributed to writing and editing the paper.

COMPETING INTERESTS

The authors declare no competing interests.